One-photon pair annihilation in pulsed plane-wave backgrounds

S. Tang,* A. Ilderton, and B. King
Centre for Mathematical Sciences, University of Plymouth, Plymouth PL4 8AA, United Kingdom

(Received 13 September 2019; published 19 December 2019)

We study the $2 \to 1$ process of electron-positron pair annihilation to a single photon in a plane-wave background. The probability of the process in a pulsed plane wave is presented, and a locally constant field approximation is derived and benchmarked against exact results. The stricter kinematics of annihilation (compared to the $1 \to 2$ processes usually studied) leads to a stronger dependence on the incoming particle states. We demonstrate this by studying the effect that initial-state wave packets have on the annihilation probability. The effect of annihilation in a distribution of particles is studied by incorporating the process into Monte Carlo simulations.

DOI: 10.1103/PhysRevA.100.062119

I. INTRODUCTION

At the single-vertex level, the stimulated QED processes that can occur in a background electromagnetic field may be divided into the $1 \to 2$ processes, namely, nonlinear Compton (NLC) scattering [1,2] and the nonlinear Breit-Wheeler (NBW) [1,3,4] and $2 \to 1$ processes of one-photon absorption [5] and one-photon pair annihilation [5]. All of these processes are forbidden in the absence of a background.

NLC and NBW have been thoroughly studied both analytically [1,2,5–15] and through numerical implementation in particle-in-cell (PIC) codes [16,17], where they contribute to, e.g., electromagnetic cascade formation [18–24]. In this context, the $2 \to 1$ processes are entirely neglected, the usual justification being that the outgoing particle phase space of these processes is completely determined by that of the initial particles, leading to their probabilities being proportional to an initial particle density factor that suppresses the process, relative to NLC and NBW. (The theory of one-photon pair annihilation has been studied in only a handful of papers [1,5,25,26].)

A simple estimate suggests that these processes should be negligible unless one of the initial particle species has a density of the order of one particle per Compton wavelength cubed. (This is typical for, e.g., "many to few" processes, and will be made explicit in the formulas below.) This requirement for the species density ($\sim 7 \times 10^{28}$ cm^{-3}) is about 10^4 times denser than solid density ($\sim 10^{24}$ cm^{-3}). However, this should be verified by, e.g., calculation and simulation, and furthermore there are several situations in laser-plasma physics where high particle densities can occur. For example, at the boundary of an irradiated solid target [27–31], an extremely dense electron foil is compressed by ultrarelativistic lasers. Also, at very high values of the laser field intensity parameter $\xi = eE/m\omega_l \approx O(10^3)$ (where e and m denote the positron charge and mass, and E and ω_l are the laser electric field amplitude and frequency, respectively), QED cascades comprising chains of NLC and NBW processes are predicted to occur [21,22,32–36]. In such cascades, electron-positron plasmas are produced and could be compressed to densities much higher than the plasma relativistic critical density.

In this paper, we derive a numerical implementation of one-photon pair annihilation and investigate its relevance to the above situations. The paper is organized as follows. In Sec. II, we calculate the probability of annihilation to one photon, derive its locally constant field approximation (LCFA), and benchmark against exact results for a circularly polarized monochromatic field. We then present a study of the dependency of parameters for the probability and a comparison with the background two-photon process. Approximate scaling arguments are also obtained. In Sec. III, we demonstrate numerical implementations of our results and investigate the relevance of one-photon pair annihilation to laser-plasma and cascade scenarios. We conclude in Sec. IV.

II. ONE-PHOTON PAIR ANNIHILATION

Electron-positron annihilation in vacuum yields at least two photons [37,38]. However, in the presence of a background field, annihilation to one photon becomes kinematically accessible; see Fig. 1. At low background intensities, the leading-order process is again two-photon emission, but with one of the photons emitted *into* the background. Therefore, when we consider one-photon pair annihilation, we are also summing over processes that are degenerate with it, such as the (unobservable) emission back to the field [39].

Here we briefly outline the derivation of one-photon pair annihilation in pulsed plane-wave backgrounds, modeling intense laser pulses. We highlight only those parts of the calculation that differ relative to the more standard $1 \to 2$ one-vertex QED processes (a more detailed example of our derivation can be found in Ref. [24]). We use natural units $\hbar = c = 1$ throughout and the fine-structure constant is $\alpha = e^2 \approx 1/137$. The interaction scenario is set up in Fig. 2: we can study the phenomenology of a single process by considering an initial electron (positron) with momentum p^μ (q^μ) annihilates to a photon with momentum l^μ in a

*suo.tang@plymouth.ac.uk

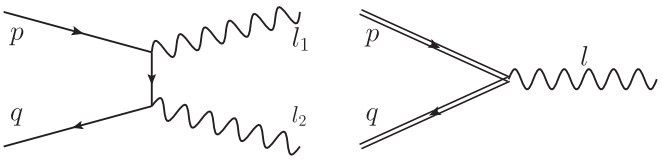

FIG. 1. Feynman diagram for pair annihilation. Left: Two-photon process in vacuum. Right: One-photon process in a field background. Double lines denote dressed Volkov states.

background laser field as shown in Fig. 2(a). However, an experimental scenario will likely involve high particle density of one species as a target, which we choose to be the electrons, and consider the positrons to be in a beam as shown in Fig. 2(b). The laser field is modeled by the potential $eA^\mu(\phi) = a^\mu(\phi) = [0, a^1(\phi), a^2(\phi), 0]$, in which $\phi = k\cdot x$, with $k = \omega_l(1,0,0,1)$ being the laser wave vector. The electron is described as a standard Volkov wave function [40],

$$\Psi_{e^-}(p) = \sqrt{\frac{m}{Vp^0}}\left(1 + \frac{\not{k}\not{a}}{2k\cdot p}\right)u_{p,\sigma} \times e^{-i[p\cdot x + \int^\phi d\phi'(\frac{p\cdot a}{k\cdot p} - \frac{a^2}{2k\cdot p})]}, \tag{1}$$

where the spinor $u_{p,\sigma}$ satisfies the relation $\sum_\sigma u_{p\sigma}\overline{u}_{p\sigma} = (\not{p} + m)/(2m)$. The positron is also described by a Volkov wave function, but we include a momentum-space wave packet $\rho(q)$ to represent a beam of positrons. Writing $\Psi_{e^+}(q)$ for the positron Volkov wave function, the positron is described by

$$\Phi_{e^+} = \int \frac{d^3q}{(2\pi)^3}\frac{m}{q^0}\rho(q)\Psi_{e^+}(q), \tag{2}$$

where ρ obeys the normalization condition

$$\int \frac{d^3q}{(2\pi)^3}\frac{m}{q^0}|\rho(q)|^2 = 1. \tag{3}$$

The S-matrix element for annihilation is

$$\mathsf{S}_{\mathrm{fi}} = ie\sqrt{\frac{2\pi}{l^0 V}}\int d^4x\,\overline{\Phi}_{e^+}\not{\epsilon}\,e^{il\cdot x}\,\Psi_{e^-}, \tag{4}$$

where ϵ_μ is the polarization of the produced photon, obeying $\epsilon\cdot\epsilon = -1$ and $l\cdot\epsilon = 0$. The probability P for annihilation is then

$$\mathsf{P} = \int \frac{V d^3l}{(2\pi)^3}\frac{1}{4}\sum_{\text{pol,spin}}|\mathsf{S}_{\mathrm{fi}}|^2, \tag{5}$$

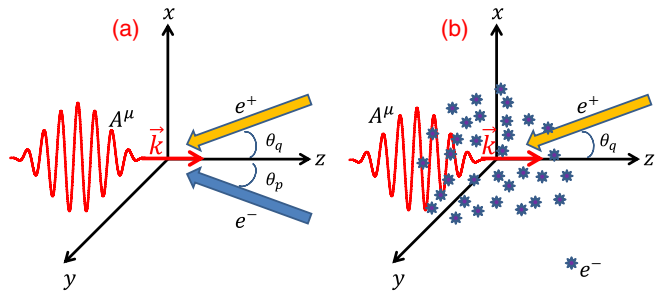

FIG. 2. Scheme of one-photon pair annihilation. (a) An electron (e^-) beam and a positron (e^+) beam collide with a laser pulse (A^μ). (b) A positron beam impinges a dense electron target.

where we sum over the polarization of the outgoing photon and average over the spins of the incoming pair. For details of the calculation, see, e.g., [39]. We find

$$\mathsf{P} = \frac{\alpha\lambda_c^3}{8\pi^2 V}\frac{m}{p^0}\int\frac{d^3q}{(2\pi)^3}\frac{m}{q^0}\frac{|\rho(\boldsymbol{q})|^2}{\eta_q\eta_l}\int d\phi_1 d\phi_2 \times\left\{1 + \frac{[a(\phi_1) - a(\phi_2)]^2}{m^2}\frac{\eta_p^2 + \eta_q^2}{4\eta_q\eta_p}\right\}e^{\frac{-i}{2\eta_l}\int_{\phi_2}^{\phi_1}d\phi'\frac{\pi_l^2}{m^2}}, \tag{6}$$

where $\eta_p = k\cdot p/m^2$, $\eta_q = k\cdot q/m^2$, $\eta_l = \eta_p + \eta_q$, and $\lambda_c = 2\pi/m$ is the electron Compton wavelength. We define the shorthand $\pi_l(\phi) = \pi_p(\phi) + \pi_q(\phi)$, and $\pi_p^\mu = p^\mu + a^\mu - (2p\cdot a + a^2)k^\mu/(2k\cdot p)$ $[\pi_q^\mu = q^\mu - a^\mu + (2q\cdot a - a^2)k^\mu/(2k\cdot q)]$ is the instantaneous four-momentum of the electron [positron] in a plane wave. Note that the probability contains the leading density factor λ_c^3/V.

A. LCFA

To derive the LCFA, we follow the usual procedure of rewriting the external-field phases in terms of an average phase $\psi = (\phi_1 + \phi_2)/2$ and an interference phase $\vartheta = \phi_1 - \phi_2$ [24], expanding the exponent to order ϑ^3:

$$\int_{\phi_1}^{\phi_2} d\phi'\pi_l^2 \to \vartheta\pi_l^2(\psi) + \frac{\vartheta^3}{24}\left[\pi_l^2(\psi)\right]'', \tag{7}$$

and the preexponent up to order ϑ^2 through the replacement $[a(\phi_1) - a(\phi_2)]^2 \to -m^2\vartheta^2\boldsymbol{\xi}^2(\psi)$, where we define the normalized electric field $\boldsymbol{\xi}$ as $\boldsymbol{a}'/m = (\boldsymbol{\xi}, 0)$. This allows us to integrate Eq. (6) over ϑ. The probability becomes

$$\mathsf{P} = \frac{\alpha\lambda_c^3}{2\pi V}\int\frac{d^3q\,m}{(2\pi)^3 q^0}|\rho(q)|^2 g(p,q,\boldsymbol{\xi}), \tag{8}$$

which has the form of an incoherent average over the positron wave packet $|\rho(q)|^2$ and the probability for one-photon annihilation of a pair with *definite* momenta p and q, which is encoded in g. The dependence on the particle momenta and the field $\boldsymbol{\xi}$ is described by

$$g(p,q,\boldsymbol{\xi}) = \frac{m}{p^0\eta_q}\int d\psi\, f(p,q,\boldsymbol{\xi}), \tag{9}$$

in which

$$f(p,q,\boldsymbol{\xi}) = \left(\frac{\chi_q^{1/3}\chi_p^{1/3}}{\chi_l^{4/3}} + \frac{\chi_p^2 + \chi_q^2}{\chi_l^2}z\right)\mathrm{Ai}(z), \tag{10}$$

where all χ variables depend on the average phase ψ via $\chi_p = \eta_p|\boldsymbol{\xi}(\psi)|$, $\chi_q = \eta_q|\boldsymbol{\xi}(\psi)|$, $\chi_l = \chi_p + \chi_q$, and $\mathrm{Ai}(z)$ is the Airy function with argument

$$z = \frac{(\pi_p + \pi_q)^2}{m^2\,\chi_l}\left(\frac{\chi_q\chi_p}{\chi_l}\right)^{\frac{1}{3}}. \tag{11}$$

Observe that the LCFA result depends not only on the quantum nonlinearity parameter $\chi_{p,q}$, but also on the local momenta of the two particles, $\pi_{p,q}$.

Comparing the derivation above with that of the LCFA for NLC [15,24] would suggest that a necessary condition for the

validity of the one-photon annihilation LCFA is

$$\frac{1+\xi^2}{2}\left(\frac{1}{\eta_q}+\frac{1}{\eta_p}\right)\gg 1. \tag{12}$$

We will see below that this parameter makes an explicit appearance. We will also see, though, that this condition is not sufficient and that wave-packet phenomena play an important role.

B. LCFA benchmarking

To benchmark the LCFA result, we consider one-photon pair annihilation in a circularly polarized monochromatic field: $\boldsymbol{\xi}(\psi)=\xi[\cos\psi,-\sin\psi,0]$, in which ξ is the coupling of matter to the background field, i.e., the "dimensionless intensity parameter" of the plane wave. Unlike the case of $1\to 2$ processes, where the LCFA can be compared straightforwardly, in $2\to 1$ processes the number of outgoing momentum integrals is not always sufficient to evaluate all momentum-conserving δ functions. However, if one of the incoming particles is in a wave-packet state, as we consider here, then all the δ functions can be evaluated and the LCFA can again be benchmarked straightforwardly.

We take our positron wave packet to be

$$|\rho(q)|^2=(2\pi)^3\frac{q^-}{m}\nu(q^-)\frac{4\ln(2)}{\pi\Delta^2 m^2}e^{-\frac{4\ln(2)}{\Delta^2 m^2}|\boldsymbol{q}^\perp-\boldsymbol{q}_i^\perp|^2}, \tag{13}$$

which is Gaussian distributed in transverse momentum with full width at half maximum Δm, while the longitudinal wave packet $\nu(q^-)$ satisfies the normalization condition, $\int_0^\infty dq^-\nu(q^-)=1$. This ansatz for the wave packet facilitates the intended comparison by matching well with the symmetries of the plane-wave background. The explicit form of $\nu(q^-)$ will not be required, as we will focus on transverse momentum dependence.

Inserting the above wave packet into Eq. (8), we can obtain the probability,

$$\mathsf{P}_\nu^{\mathrm{lcfa}}=\frac{32\pi^2\ln(2)\delta(0)\alpha}{Vk^0p^0\Delta^2}\int_0^1\frac{dv\,\nu(q^-)}{(1-v)^2}h_l(v), \tag{14}$$

where $\delta(0)=\int d\psi/(2\pi)$, $v=\eta_q/\eta_l$, and

$$h_l(v)=\frac{1}{2\pi}\int d^2\boldsymbol{r}\int_0^{2\pi}d\psi\,e^{-\frac{4\ln(2)}{\Delta^2 u}|\boldsymbol{r}-\boldsymbol{r}_i|^2}\times v^2\left[\frac{u}{(v\chi_p)^{2/3}}+(1+u^2)z\right]\mathrm{Ai}(z), \tag{15}$$

with the definitions

$$\boldsymbol{r}=\frac{\boldsymbol{q}^\perp}{m}\sqrt{u}-\frac{\boldsymbol{p}^\perp}{m}\sqrt{\frac{1}{u}},\quad \boldsymbol{r}_i=\frac{\boldsymbol{q}_i^\perp}{m}\sqrt{u}-\frac{\boldsymbol{p}^\perp}{m}\sqrt{\frac{1}{u}},$$

where $u=\eta_p/\eta_q$.

We find the annihilation probability in a circularly polarized monochromatic wave to be

$$\mathsf{P}_\nu^{\mathrm{mono}}=\frac{32\pi^2\ln(2)\delta(0)\alpha}{Vk^0p^0\Delta^2}\int_0^1\frac{dv\,\nu(p^-)}{(1-v)^2}h_a(v), \tag{16}$$

in which h_a contains a sum over harmonics,

$$h_a(v)=\sum_{n\geqslant n_v}^{\infty}T_n, \tag{17}$$

in which the lower harmonic bound n_v is defined to be

$$n_v=\frac{1+\xi^2}{2\eta_p v} \tag{18}$$

and is exactly equal to the parameter introduced in (12). Hence we already expect, as for other processes, that the LCFA will be unable to reproduce low harmonic structure. This will be confirmed below. In (17), we also have

$$T_n(v)=\int_{-\pi}^{\pi}d\varphi\,e^{-\frac{4\ln(2)}{\Delta^2 u}(\boldsymbol{r}_n-\boldsymbol{r}_i)^2}H_n, \tag{19}$$

where φ is the angle between $\boldsymbol{r}_n$ and $\boldsymbol{r}_i$, $\cos(\varphi)=\boldsymbol{r}_n\cdot\boldsymbol{r}_i/(r_n r_i)$, $r_i:=|\boldsymbol{r}_i|$ is a function of only initial variables, and

$$r_n^2=|\boldsymbol{r}_n|^2=2n\eta_p\frac{v-v^*}{v(1-v)},\quad v^*=\frac{1+\xi^2}{2n\eta_p},$$

and n is the harmonic number,

$$H_n=\frac{\xi^2}{4}\left[\frac{n^2-s_n^2}{s_n^2}J_n^2(s_n)+J_n'^2(s_n)\right]\frac{1-2v^2u}{v^2u}+\frac{J_n^2(s_n)}{2},$$

where $J_n(s_n)$ is the Bessel function of the first kind, with argument

$$s_n=\frac{\xi^2\sqrt{2n\eta_p(v-v^*)}}{\chi_p v}.$$

We compare, in Fig. 3, the LCFA result given by Eq. (15) with the exact monochromatic result given by Eq. (17), for various parameters and wave packets of different widths. In the figure, the LCFA is represented by dashed lines and the monochromatic result by solid lines.

In Fig. 3(a), the LCFA result for a flat wave packet matches well with the exact calculation when the field intensity is relatively strong; notice that the LCFA cannot reproduce the low-n harmonic structure visible at, e.g., $\xi=1$ (red lines), as expected from other investigations of the LCFA [41]; see, also, [15,24,42]. For pair annihilation, we find a similar dependency on the minimum harmonic as for the time-reversed process of NBW pair creation [1]. There is a *lower bound* n_v on the harmonic number which *increases* with intensity; as the LCFA does better at reproducing results where large numbers of higher harmonics contribute [15,24,41,42], the quality of the LCFA improves quickly here, being extremely accurate already for $\xi=4$ (magenta lines). Consequently, a similar effect results from decreasing η_p: this also raises the harmonic lower bound, leading to weaker harmonic structure, meaning that the LCFA gives a better approximation of the monochromatic result even at low laser intensities. This is confirmed in Figs. 3(b) and 3(c).

We also highlight the behavior at $v=1$ in Fig. 3(a) for the flat wave packet, where $h_l, h_a\to\infty$. This divergence comes from the superposition of an infinite number of states with the same longitudinal momentum. However, this behavior is different when the included wave packet has a finite momentum bandwidth. As we compare, in order, Figs. 3(a)–3(d), the wave packet becomes narrower and the exact result oscillates rapidly as $v\to 1$, with the oscillating structure spreading to lower v as the wave packet narrows. These rapid oscillations result from an interplay between the harmonics and the Gaussian wave packet: the contribution of each harmonic is

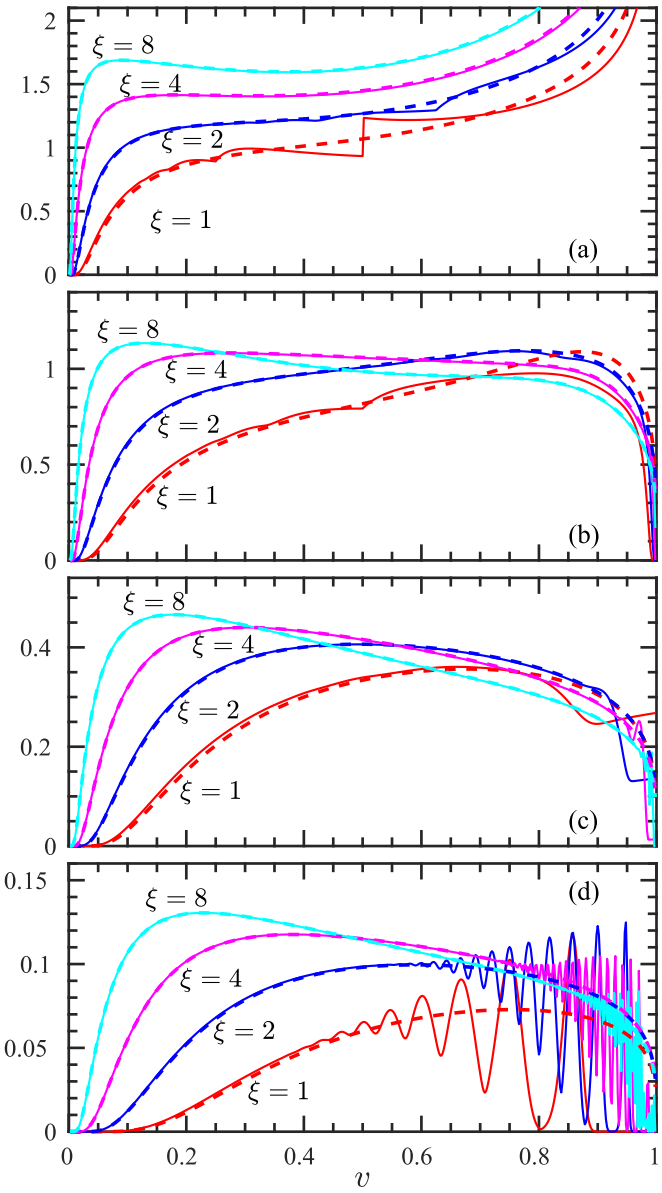

FIG. 3. Benchmarking the LCFA $h_l^{1/4}(v)$ against the exact result $h_a^{1/4}(v)$. (a) $\Delta = \infty$, $\eta_p = 2$. (b) $\Delta = 20$, $\eta_p = 1$. (c) $\Delta = 2$, $\eta_p = 0.5$. (d) $\Delta = 0.25$, $\eta_p = 0.2$. Dashed (solid) lines are for LCFA (exact) result. Red lines: $\xi = 1$; green lines: $\xi = 2$; magenta lines: $\xi = 4$; and blue lines: $\xi = 8$. In (b)–(d), $q_{i,x} = -p_x = \xi$ and $q_{i,y} = p_y = 0$.

effectively localized by the narrow wave packet. The dominant contribution from each harmonic originates from the condition $(\boldsymbol{r}_i - \boldsymbol{r}_n)^2 = 0$, as can be seen from the exponent in Eq. (19). This can be solved for v, showing that the nth harmonic H_n will be restricted to contribute around $v \simeq v_n$, where

$$v_n := \frac{1 + 2\xi^2}{2\eta_p n}. \tag{20}$$

Here we have used that $\boldsymbol{p}^\perp = -\boldsymbol{q}_i^\perp$ and $|\boldsymbol{p}^\perp| = \xi$ as in Fig. 3. To see these effects explicitly, we zoom in to the peak structure for $\xi = 1$ (red solid line) in Fig. 3(d) and highlight, in Fig. 4, the contribution from different harmonics. As predicted, the

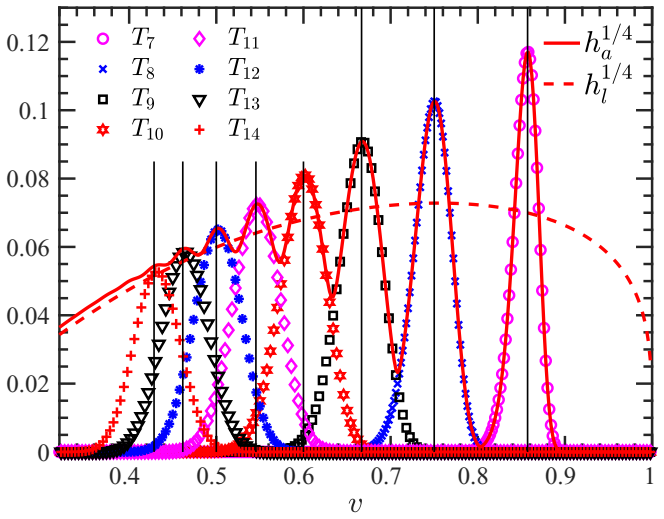

FIG. 4. Harmonic peak structure. Here we zoom in to the peak structure of the red line for $\xi = 1$ in Fig. 3(d), and also plot the individual harmonic contributions $T_n^{1/4}$. The vertical black lines denote the location v_n of each harmonic, as in Eq. (20). The harmonic order changes from 7 to 14 as we go from right to left.

nth harmonic is highly localized around the point $v = v_n$. Also, the harmonics that significantly contribute are substantially above the lower bound n_v. It is clear from Fig. 4 that the separation of the harmonic contributions, due to the wave packet, is responsible for the appearance of the oscillatory structure as the wave-packet width decreases. Furthermore, the LCFA result fails to manifest this peak structure at all. As v decreases, the harmonic peaks overlap and can be matched better by the LCFA, but this agreement is again lost as the wave packet continues to narrow and the harmonic peaks become much sharper, as in Figs. 3(c) and 3(d). [We also find that the oscillation frequency increases with the increase of the laser intensity; see Fig. 3(d).] We conclude that the LCFA is unable to reproduce the $2 \to 1$ physics of narrow (momentum-space) wave packets.

C. Phenomenology

In this section, we study the dependence of one-photon pair annihilation on the incident particle parameters, assuming plane-wave initial states. The particle momenta are expressed in spherical polar coordinates as depicted in Fig. 2(a): $\boldsymbol{p} = -(E_p^2 - m^2)^{1/2}[\sin\theta_p \cos\varphi_p, \sin\theta_p \sin\varphi_p, \cos\theta_p]$ and $\boldsymbol{q} = -(E_q^2 - m^2)^{1/2}[\sin\theta_q \cos\varphi_q, \sin\theta_q \sin\varphi_q, \cos\theta_q]$, where E_p, θ_p, φ_p (E_q, θ_q, φ_q) are the incident energy, polar and azimuthal angle of the electron (positron). We analyze one cycle of a monochromatic field with (i) linear polarization $a^\mu(\psi) = m\xi[0, \cos\psi, 0, 0]$ and (ii) circular polarization $a^\mu(\psi) = m\xi[0, \sin\psi, \cos\psi, 0]$. For linear polarization, we consider the collision to take place in the incident plane of the laser background.

It is helpful for what follows to understand where the dominant contributions to $f(p, q, \boldsymbol{\xi})$ in Eq. (10) come from, in terms of phase ψ and as a function of the particle momenta. The pair should have similar energy $E_p \approx E_q$, and we find that $f(p, q, \boldsymbol{\xi})$ exhibits one (two) sharp peak per laser cycle for

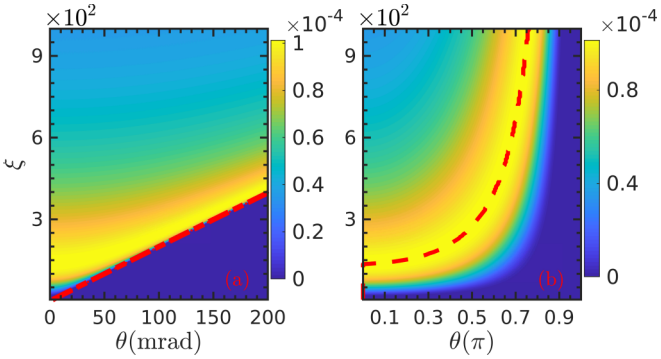

FIG. 5. Parametric dependency of $g(p, q, \xi)$ on the laser amplitude ξ and the particles' incident angle θ_p, θ_q. (a) $\theta_p = -\theta_q =: \theta$. (b) $\theta_p = \theta_q =: \theta$. The red dot-dashed line in (a) is $\xi = |\boldsymbol{p}| \sin(\theta)/m$, and the red dashed line in (b) corresponds to $\eta_p \xi = 4/3$. The particle energy is fixed, $E_p = E_q = 2000$ m, and a laser is linearly polarized, with frequency $\omega_l = 1.24$ eV.

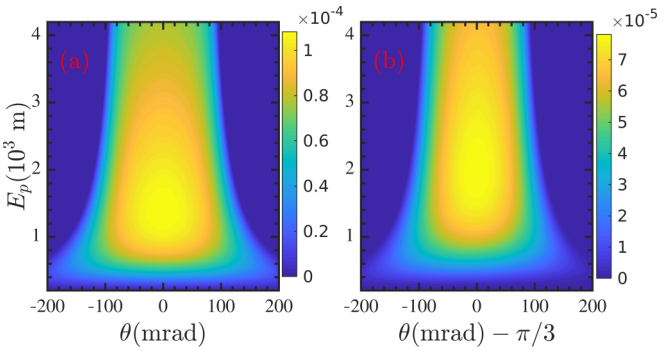

FIG. 6. Parametric dependency of $g(p, q, \boldsymbol{\xi})$ on the incident parameters of the positron. (a) $\theta_p = 0$, $E_p = 1360m$. (b) $\theta_p = \pi/3$, $E_p = 1360m$. The laser amplitude is $\xi = 100$ and the other parameters are the same as in Fig. 5.

circular (linear) polarization. These peaks appear at the points where $\boldsymbol{\pi}_p(\psi)$ is parallel to $\boldsymbol{\pi}_q(\psi)$. For linear polarization, if $\theta_p = \theta_q$, the peaks appear at the points where $a(\psi) = 0$, and if $\theta_p = -\theta_q = \theta$, the peaks appear at $m\xi \cos\psi = E_p \sin\theta$, where $E_p \gg m$ is used. For circular polarization, a peak appears at $\boldsymbol{a}(\psi) = E_p[\sin\theta_p \cos\varphi_p, \sin\theta_p \sin\varphi_p, 0]$, if $\boldsymbol{p}^\perp + \boldsymbol{q}^\perp = 0$. Because the electromagnetic (EM) field rotates in a circularly polarized background, these acceptance peaks are much narrower than for a linearly polarized background. Thus one-photon pair annihilation is much more effective in a linearly polarized laser.

Figure 5 shows the dependency of the integrated expression $g(p, q, \boldsymbol{\xi})$ from Eq. (9) on the laser amplitude ξ and the particles' incident angle θ. In Fig. 5(a), we can see that in order that the process is not strongly suppressed, the laser intensity must be increased for larger values of incident collision angle θ. The reason for this is that the laser field must be strong enough to make the local momenta of the pair particles, $\boldsymbol{\pi}_p$ and $\boldsymbol{\pi}_q$, parallel to one another. If the pair particles propagate parallel to one another and collide head-on with the laser pulse, there is an optimal value of ξ, above which the probability then decreases. This is because, even though the strength of the interaction is increased, there is a suppression at high intensities due to a narrowing of the effective phase width in the integrand $f(p, q, \boldsymbol{\xi})$. For a high enough intensity, the most probable setup for one-photon pair annihilation is actually when the collision is not directly head-on, as shown in Fig. 5(b). This is because one-photon pair annihilation achieves the largest probability if the quantum nonlinearity parameter $\chi = 4/3 \sim [1 + \cos(\theta)]\xi$ [this will be further commented on in the next section and Eq. (24)].

In Fig. 6, we show the dependency of $g(p, q, \boldsymbol{\xi})$ on the incident parameters (E_q, θ_q) of the positron for the given laser amplitude $\xi = 100$ and electron incident parameters [$E_p = 1360m$, $\theta_p = 0$ in Fig. 6(a) and $\theta_p = \pi/3$ in Fig. 6(b)]. As we can see, the largest probability could be obtained if the pair particles have the same initial parameters ($\theta_p \approx \theta_q$, $E_p \approx E_q$). With a relative larger incident angle in Fig. 6(b), the process would be less effective because $\chi_p \sim 1 + \cos(\theta)$ is smaller.

In Fig. 7, we consider the dependency of $g(p, q, \boldsymbol{\xi})$ on the particle energy and laser amplitude with head-on collisions, $\theta_p = \theta_q = 0$. As shown in Fig. 7(a), a stronger laser field could induce larger annihilation probability and also decrease the requirement for the particle energy (see the red dotted line). This is because the probability has a maximum at $\chi_p = 2/3$ [this will be discussed further in Eq. (25)], and in Fig. 7(b), the maximal probability for a given laser field ξ increases with a stronger laser field.

D. Approximations

To understand the dependency of one-photon pair annihilation on experimental parameters, it is useful to approximate the phase integral in Eq. (9).

To simplify the calculation, in this section we consider two cases, corresponding to Figs. 5(a) and 5(b), respectively. First of all, we assume a head-on collision $\theta_p = \theta_q = 0$ [Fig. 5(a)] with a linearly polarized monochromatic laser field $\boldsymbol{\xi}(\psi) = \xi[\sin(\psi), 0, 0]$, and consider an integration over one cycle of this field. The argument z of the Airy function becomes

$$z = z_m[1 + \xi^2 \cos^2(\psi)] \sin^{-2/3}(\psi), \tag{21}$$

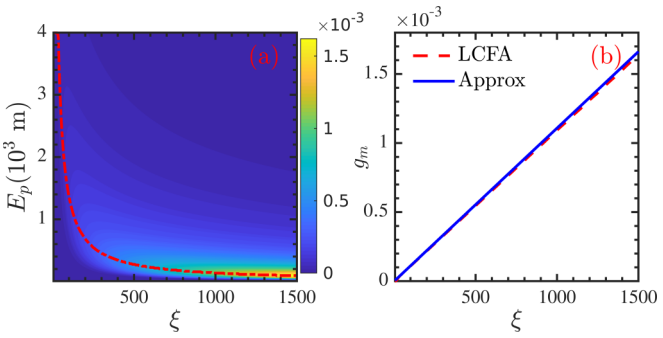

FIG. 7. (a) Parametric dependency of $g(p, q, \xi)$ on the particle energy $E_p = E_q$ and laser amplitude ξ. The red dot-dashed line denotes the particle energy giving the largest $g(p, q, \xi)$. (b) Largest $g(p, q, \xi)$ for a given laser intensity ξ. The red dashed line corresponds to the red dot-dashed line in (a) and the blue line comes from the approximation given by Eq. (25). Head-on collision ($\theta_p = \theta_q = 0$) is applied, and the other parameters are the same as in Fig. 5.

where $z_m = (\eta_p + \eta_q)^{2/3}/(\eta_q\eta_p\xi)^{2/3}$. The leading contribution comes when $a(\psi) \approx 0$ and z is at a minimum. With $\xi \gg 1$, the Airy functions decay exponentially as ψ deviates from the values $\psi = \pi/2,\ 3\pi/2$; hence, in order to obtain the dominant contributions, we Taylor expand z in ψ, to the order of ψ^2, around the corresponding points. By then integrating over ψ in Eq. (9), we arrive at

$$g(p,q,\xi) \approx \frac{2m}{p^0\eta_q}(\eta_p+\eta_p)^{-\frac{4}{3}}(\eta_p\eta_q)^{\frac{1}{3}}\xi^{-\frac{5}{3}}\frac{\pi}{\sqrt{z_m}} \times\left[\left(1+\Gamma-\frac{1+2\Gamma}{6\xi_0^2}\right)2^{\frac{2}{3}}\mathrm{Ai}^2(2^{-\frac{2}{3}}z_m) +\frac{1+2\Gamma+6\xi_0^2\Gamma}{3\xi_0^2 z_m}2^{\frac{1}{3}}\mathrm{Ai}'^2(2^{-\frac{2}{3}}z_m)\right], \quad (22)$$

where $\Gamma = \Gamma(p,q) = (\eta_p^2+\eta_q^2)/(2\eta_q\eta_p)$. If $2^{-\frac{2}{3}}z_m \gg 1$, we can obtain

$$g(p,q,\xi) \approx \frac{m}{p^0\eta_q}\frac{\eta_p\eta_q}{(\eta_p+\eta_q)^2}\frac{1+2\Gamma}{\xi}\exp\left(-\frac{2}{3}z_m^{\frac{3}{2}}\right), \quad (23)$$

and if $p = q$, $g(p,q,\xi)$ can be further simplified,

$$g(p,q,\xi) \approx \frac{3m}{4p^0}\frac{1}{\chi_m}\exp\left(-\frac{4}{3\chi_m}\right), \quad (24)$$

where $\chi_m = \eta_p\xi$. [This is reminiscent of the famous $\exp(-8/3\chi_l)$ scaling of the time-reversed process of NBW pair creation in a constant crossed field in the asymptotic limit $\chi_l \ll 1$.]

We can perform the same analysis for $\theta_p = \theta_q = \theta$ [Fig. 5(b)]. Using the same approximation as in Eq. (24), we see that for a given particle energy $E_p = E_q$, $g(p,q,\xi)$ has a maximum if $\chi_m = 4/3$ [corresponding to the green dashed line in Fig. 5(b)], and for a given laser amplitude ξ, $g(p,q,\xi)$ has a maximum if $\chi_m = 2/3$ [see the blue line in Fig. 7(b)]. $g(p,q,\xi)$ then takes the value

$$g_{\mathrm{m}} = \frac{27}{8}\frac{\omega_l\xi}{m}e^{-2}, \quad (25)$$

where we have made use of the relation $k\cdot p \approx 2\omega_l p^0$ if $p^0 \gg 1$ in a head-on collision.

The approximations above are for a single cycle of a monochromatic background, but the same approximation can be made for longer pulses by summing over contributions where $a(\psi_i) = 0$:

$$g(p,q,\xi) \approx \frac{m}{2p^0}\frac{\eta_p}{(\eta_p+\eta_q)^2}\sum_i\frac{1+2\Gamma}{|\boldsymbol{\xi}(\psi_i)|}e^{-\frac{2}{3}z_m^{3/2}(\psi_i)}. \quad (26)$$

To demonstrate the validity of the approximation, we show in Fig. 8 the comparison between the numerical calculation of Eq. (9) and the approximation given by Eq. (23). As we can see, the approximation works well in a broad parameter region, with the discrepancy growing in the extremely high-field and high-energy region as $z_m \gtrsim 1$.

E. Comparison with zero-field two-photon pair annihilation

Based on Eq. (8) and the definition of the cross section, $\sigma = (1/|v_{\mathrm{rel}}|n_{e^-})d\mathsf{P}/dt$ [43], where t is time and $|v_{\mathrm{rel}}| = (p^0q^0)^{-1}\sqrt{(p\cdot q)^2-m^4}$ is the relative velocity between the pair particles, we can easily calculate the cross section for one-photon pair annihilation,

$$\sigma_1 = \frac{2\alpha\lambda_c^2}{\sqrt{\kappa^2-4\kappa}}\frac{1}{2\pi N_l}\int d\psi\, f(p,q,\boldsymbol{\xi}), \quad (27)$$

where $\kappa = (p+q)^2/m^2$ is the scaled Mandelstam invariant, N_l is the number of laser cycles, and we replace the volume

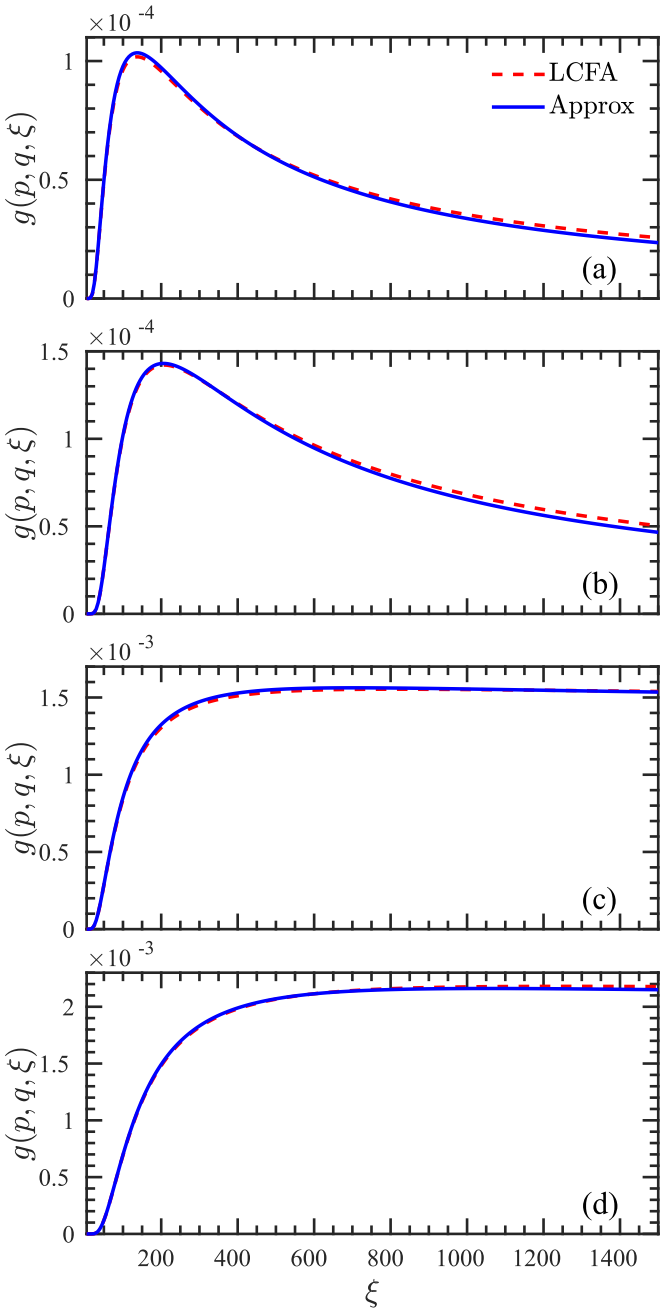

FIG. 8. Comparison between the numerical calculation of Eq. (9) and the approximation given by Eq. (23) for a head-on collision. In (a) and (b), the results for one cycle of a monochromatic laser pulse $\boldsymbol{\xi}(\psi) = \xi\,[\sin(\psi), 0, 0]$ are displayed. In (c) and (d), the cases of a long laser pulse $\boldsymbol{\xi}(\psi) = \xi\,[\sin(\psi), 0, 0]\,\mathrm{sech}^2[\psi/(\omega_l T)]$, $\omega_l = 1.24$ eV, and $T = 5T_l$, $T_l = 2\pi/\omega_l$ are presented. In (a) and (c), $E_p = E_q = 2000m$; in (b) and (d), $E_p = 2000m$, $E_q = 1000m$.

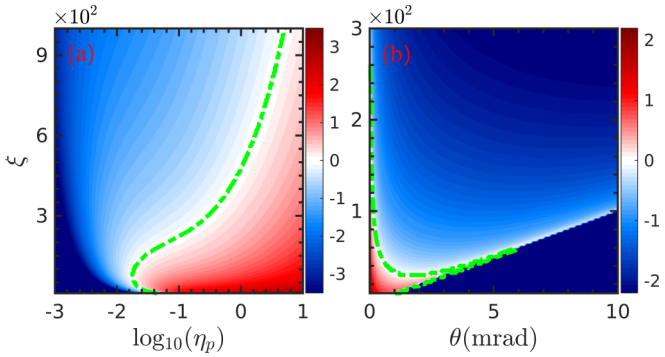

FIG. 9. Ratio between σ_1 and σ_2: $\ln(\sigma_1/\sigma_2)$. (a) $\theta_p = \theta_q = 0$, $E_p = E_q$. (b) $\theta_p = -\theta_q = \theta$, $E_p = E_q = 10^4 m$, $\omega_l = 4.65$ eV. The green dot-dashed lines denote $\sigma_1 = \sigma_2$. $N_l = 1$, and the other parameters are the same as in Fig. 5.

factor $1/V$ in Eq. (8) with the electron density n_{e^-}. (Here, an "evening out" of the instantaneous cross section is performed by averaging over the phase of the incident laser pulse.) The cross section for the two-photon annihilation process in vacuum is calculated in Ref. [38],

$$\sigma_2 = \frac{\alpha^2\lambda_c^2}{2\pi}\frac{1}{\kappa-4}\left[-\frac{\kappa+4}{\kappa}\sqrt{\frac{\kappa-4}{\kappa}} + \ln\left(\frac{\kappa-2}{2}+\sqrt{\frac{\kappa^2}{4}-\kappa}\right)\frac{\kappa^2+4\kappa-8}{\kappa^2}\right]. \quad (28)$$

In Fig. 9, we compare the ratio σ_1/σ_2 of the cross sections for the two processes. As we can see, with small incident angle $\theta \ll 1$, the laser-assisted one-photon pair annihilation can be more probable than the two-photon annihilation in vacuum, especially when we have head-on collision $\theta = 0$ with the laser pulse. To measure this in experiment, we see that one would have to resolve the angular spectra of annihilation photons, where, in the small-angle region, one-photon annihilation from within the pulse can exceed two-photon zero-field annihilation.

III. NUMERICAL IMPLEMENTATION

In this section, we combine our analytical calculations with numerical implementation. To consider the number of one-photon pair-annihilation events in realistic situations, we specify the positron momentum distribution to be $|\rho(q)|^2 = (2\pi)^3(q^0/m)\delta^{(3)}(\boldsymbol{q}-\boldsymbol{q}_i)$, which clearly fulfills the normalization condition given by Eq. (3). The number N_a of positron annihilation events in the interaction of N_{e^+} incident positrons with a dense electron target and a laser pulse is then

$$N_a = N_{e^+} n_{e^-} \lambda_c^3 \frac{\alpha}{2\pi}\frac{m}{p^0\eta_q}\int d\psi\, f(p,q,\boldsymbol{\xi}). \quad (29)$$

This number of events is suppressed by the electron density factor, which is small unless there is, on average, one electron per Compton wavelength cubed. (This would correspond to a density of $\sim 7\times 10^{28}$ cm^{-3}, more than 10^4 times higher than solid density $\sim 10^{24}$ cm^{-3}.) In the following, we consider two example applications of one-photon pair annihilation.

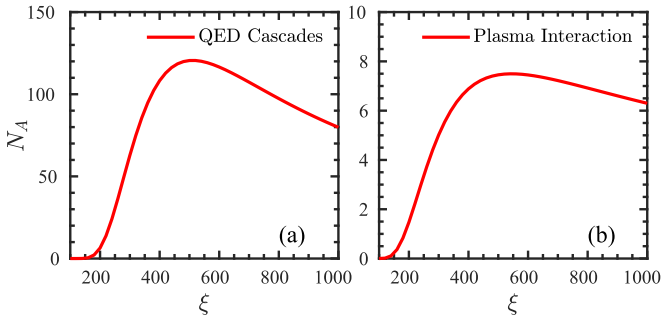

FIG. 10. Number of annihilation events in (a) QED cascades and (b) a laser-plasma interaction. A linearly polarized laser pulse, $\boldsymbol{\xi}(\psi) = \xi\,\mathrm{sech}^2[\psi/(\omega_l T)]\,[\sin(\psi), 0, 0]$, is employed where $T = 5T_l$, $\omega_l = 1.55$ eV, and $T_l = 2\pi/\omega_l$.

A. QED cascade and laser-plasma interaction

We first consider one-photon pair annihilation in QED cascades. In Ref. [32], the typical particle density in a QED cascade was given as approximately equal to the relativistic critical density $n_{e^+} = n_{e^-} \approx \xi n_c$, in which $n_c = \omega_l^2 m/4\pi$ is the plasma critical density. The typical particle energy in the cascade is around $E_p \approx E_q \approx m\xi$. Given these parameters, we show in Fig. 10(a) the number of pair annihilations in the volume of one laser wavelength cubed. In the calculation, the number of positrons is $N_{e^+} \approx \xi n_c \lambda_l^3$. As we can see, the number of annihilations is, at best, six orders of magnitude smaller than the initial positron number. We thus conclude that one-photon annihilation will have a negligible effect on QED cascades.

Another scenario in which a high electron density can arise is the irradiation of a solid plasma with an intense laser pulse [28,31]. At the plasma surface, an extreme density electron foil, with the typical density $n_{e^-} \sim \xi^2 n_c$ and energy $E_p \approx \xi m$, can be compressed. We consider the number of annihilations when a beam of $N_{e^+} \approx 10^8$ positrons with $E_q = 2000m$ is fired at the electron foil. Figure 10(b) shows calculation results for the number of annihilation events during this laser-plasma interaction. Again, this number is many orders of magnitude lower than the initial number of positrons, and as for cascades, we conclude that one-photon pair annihilation is negligible.

We note that our calculations neglect the influence of the particle direction and assume all the particles move head-on with the laser pulse, in order to consider the most optimistic situation for one-photon pair annihilation. When more experimentally realizable parameters are considered, the number of one-photon pair-annihilation events could be much smaller than the estimated numbers.

B. Incorporation in PIC

The $1 \to 2$ quantum processes of NLC and NBW are now commonly included within the contemporary particle-in-cell (PIC) framework [16,17], while the $2 \to 1$ process of one-photon pair annihilation (and one-photon absorption [39]) is neglected. To incorporate annihilation into the standard PIC algorithm, we use the so-called probability "rate" [cf. Eqs. (8)–(10)]:

$$\frac{d\mathsf{P}}{dt} = \alpha\lambda_c^2 n_{e^-}\frac{m^2}{\pi_p^0\pi_q^0} f(p,q,\boldsymbol{\xi}), \quad (30)$$

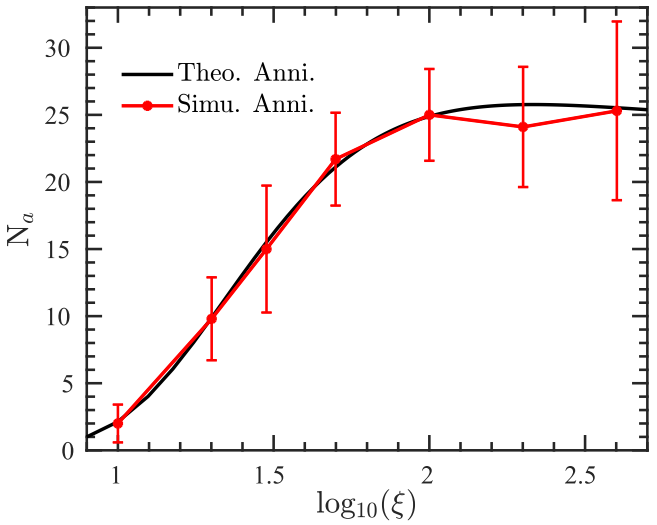

FIG. 11. Numerical simulations. Black line: theoretical number of annihilations. Red line with error bars: simulation results for the number of annihilations, averaged over 40 runs, with the error bar denoting the standard deviation. The laser pulse is the same as in Fig. 10, except $\omega_l = 4.65$ eV.

which can be implemented in the standard PIC algorithm as it depends only on local parameters. In each time step Δt, the probability for one positron annihilated in the jth pseudopositron is

$$\mathsf{P}_j = w_j \Delta t \sum_i \frac{w_i}{\Delta V} \frac{\alpha \lambda_c^2 m^2}{\pi^0_{p_i} \pi^0_{q_j}} f(p_i, q_j, \xi) = \sum_i \mathsf{P}_{i,j}, \quad (31)$$

where we sum over all the electrons i in the same grid cell as the jth pseudopositron, ΔV is the volume of the cell, and $w_{i,j}$ are the particle weights. A Monte Carlo method is applied to describe the one-photon pair-annihilation process semiclassically. Two random numbers r_1 and r_2 in [0,1] are generated to determine whether an annihilation occurs and to choose the momentum of the photon. For each pseudopositron j, an annihilation event is accepted if $r_1 < \mathsf{P}_j$, and then the momentum of the produced photon is calculated using the momentum of the kth pseudoelectron, if $\sum_{i<k-1} \mathsf{P}_{i,j}/\mathsf{P}_j < r_2 \leqslant \sum_{i<k} \mathsf{P}_{i,j}/\mathsf{P}_j$. Because the probability is extremely small, we can ignore the decrease of the particle weight induced by one-photon pair annihilation.

To demonstrate, we implement our method in a single particle code, i.e., we neglect possible plasma effects [20]. The particle beams have the initial conditions $N_{e^+} = 10^{11}$, $n_{e^-} = 10^{25}$ cm^{-3}, $E_p = E_q = 2000m$, $\theta_p = \theta_q = 0$, and the beam length $0.01\lambda_l$, and the size of the grid cell is $\Delta V = \Delta z \pi R^2$, where $\Delta z = 2 \times 10^{-4} \lambda_l$ and the transverse width of the laser beam is $R = 5\lambda_l$. As shown in Fig. 11, the simulated number of annihilations (red line) matches well with the theoretical result (black line).

In our numerical examples, in order to obtain an appreciable number of one-photon pair annihilations, we have considered a large number of positrons and an extremely dense electron beam. To obtain a prediction for a smaller number of initial positrons and a more realistic less-dense electron beam, the number of one-photon pair-annihilation events can be scaled from the simulation result based on the ratio of positron number and electron density,

$$N'_a = N_a \frac{N'_{e^+} n'_{e^-}}{N_{e^+} n_{e^-}} N_{\mathsf{sim}}, \quad (32)$$

where N_{sim} is the number of simulations. To prove this, we decrease the positron number to $N'_{e^+} = 10^9$ and the electron density to $n'_{e^-} = 10^{23}$ cm^{-3}, and repeat the simulations $N_{\mathsf{sim}} = 2 \times 10^5$. We observe $N'_a = 493$ one-photon pair annihilation for $\xi = 100$, which matches the predicted number 497.6 from the annihilation number $N_a = 24.88$ at $\xi = 100$ in the black line in Fig. 11.

This method can also be simply extended to realistic situations with specific momentum distributions because of the way the momentum part of the wave packet factorizes into the total expression; see Eq. (8). If we consider a simulation with the positron momentum distribution $|\rho(q)|^2$, we can, in principle, split it into a set of simulations with different positron momenta q and number $N_{e^+}|\rho(q)|^2$, and then sum the results N_a in each case. Based on this point, even though rapid oscillations appear in the exact result in Fig. 3, it is reasonable to implement the LCFA result in a standard PIC code because the LCFA effectively averages across these oscillations when implemented in this way.

IV. CONCLUSION

We have analysed one-photon electron-positron pair annihilation in a plane-wave background. We derived the locally constant field approximation (LCFA) for this process and benchmarked it against the exact result for a circularly polarized monochromatic background. As one may expect on the basis of LCFA results for NLC, the LCFA was found to be incapable of reproducing harmonic structure. However, an additional shortcoming of the LCFA was identified: the LCFA result cannot reproduce the physics of narrow wave packets, which manifested here as a highly oscillatory structure in the high-energy region. Further work is needed to identify sufficient conditions for the applicability of the LCFA when quantum wave packets are included in calculations.

We obtained simple scaling relations for annihilation in various setups and compared the one-photon annihilation cross section in a plane wave with the cross section of two-photon pair annihilation in vacuum. The one-photon process can be dominant for small-angle scattering in the head-on configuration.

Using numerical simulations based on the LCFA, we were able to confirm that one-photon pair annihilation will have a negligible effect on QED cascades and certain laser-plasma interactions at realizable particle densities. We also showed that annihilation can be included in large-scale numerical simulation frameworks, benchmarking our results against a particle-in-cell (PIC) simulation.

ACKNOWLEDGMENT

We thank A. J. Macleod for useful discussions. The authors are supported by the EPSRC, Grant No. EP/S010319/1.

[1] A. I. Nikishov and V. I. Ritus, Sov. Phys. JETP **19**, 529 (1964).
[2] L. S. Brown and T. W. B. Kibble, Phys. Rep. **133**, A705 (1964).
[3] H. R. Reiss, J. Math. Phys. **3**, 59 (1962).
[4] V. B. Berestetskii, L. D. Landau, E. M. Lifshitz, and L. Pitaevskii, *Quantum Electrodynamics*, Vol. 4 (Butterworth-Heinemann, Oxford, UK, 1982).
[5] V. I. Ritus and J. Russ. Laser Res. **6**, 497 (1985).
[6] M. Boca and V. Florescu, Phys. Rev. A **80**, 053403 (2009).
[7] C. Harvey, T. Heinzl, and A. Ilderton, Phys. Rev. A **79**, 063407 (2009).
[8] D. Seipt and B. Kämpfer, Phys. Rev. A **83**, 022101 (2011).
[9] T. Nousch, D. Seipt, B. Kämpfer, and A. Titov, Phys. Lett. B **715**, 246 (2012).
[10] F. Mackenroth and A. Di Piazza, Phys. Rev. A **83**, 032106 (2011).
[11] B. King, H. Gies, and A. Di Piazza, Phys. Rev. D **86**, 125007 (2012).
[12] C. N. Harvey, A. Gonoskov, M. Marklund, and E. Wallin, Phys. Rev. A **93**, 022112 (2016).
[13] T. Heinzl, A. Ilderton, and B. King, Phys. Rev. D **94**, 065039 (2016).
[14] V. Dinu, C. Harvey, A. Ilderton, M. Marklund, and G. Torgrimsson, Phys. Rev. Lett. **116**, 044801 (2016).
[15] A. Di Piazza, M. Tamburini, S. Meuren, and C. H. Keitel, Phys. Rev. A **98**, 012134 (2018).
[16] A. Gonoskov, S. Bastrakov, E. Efimenko, A. Ilderton, M. Marklund, I. Meyerov, A. Muraviev, A. Sergeev, I. Surmin, and E. Wallin, Phys. Rev. E **92**, 023305 (2015).
[17] T. D. Arber, K. Bennett, C. S. Brady, A. Lawrence-Douglas, M. G. Ramsay, N. J. Sircombe, P. Gillies, R. G. Evans, H. Schmitz, A. R. Bell *et al.*, Plasma Phys. Control. Fusion **57**, 113001 (2015).
[18] A. R. Bell and J. G. Kirk, Phys. Rev. Lett. **101**, 200403 (2008).
[19] A. M. Fedotov, N. B. Narozhny, G. Mourou, and G. Korn, Phys. Rev. Lett. **105**, 080402 (2010).
[20] N. V. Elkina, A. M. Fedotov, I. Y. Kostyukov, M. V. Legkov, N. B. Narozhny, E. N. Nerush, and H. Ruhl, Phys. Rev. ST Accel. Beams **14**, 054401 (2011).
[21] C. P. Ridgers, C. S. Brady, R. Duclous, J. G. Kirk, K. Bennett, T. D. Arber, A. P. L. Robinson, and A. R. Bell, Phys. Rev. Lett. **108**, 165006 (2012).
[22] B. King, N. Elkina, and H. Ruhl, Phys. Rev. A **87**, 042117 (2013).
[23] S. Tang, M. A. Bake, H.-Y. Wang, and B.-S. Xie, Phys. Rev. A **89**, 022105 (2014).
[24] A. Ilderton, B. King, and D. Seipt, Phys. Rev. A **99**, 042121 (2019).
[25] A. I. Voroshilo, E. A. Padusenko, and S. P. Roshchupkin, Laser Phys. **20**, 1679 (2010).
[26] A. Ilderton, P. Johansson, and M. Marklund, Phys. Rev. A **84**, 032119 (2011).
[27] A. P. L. Robinson, P. Gibbon, M. Zepf, S. Kar, R. G. Evans, and C. Bellei, Plasma Phys. Control. Fusion **51**, 024004 (2009).
[28] T. Schlegel, N. Naumova, V. Tikhonchuk, C. Labaune, I. Sokolov, and G. Mourou, Phys. Plasmas **16**, 083103 (2009).
[29] A. A. Gonoskov, A. V. Korzhimanov, A. V. Kim, M. Marklund, and A. M. Sergeev, Phys. Rev. E **84**, 046403 (2011).
[30] S. Tang, N. Kumar, and C. H. Keitel, Phys. Rev. E **95**, 051201(R) (2017).
[31] S. Tang and N. Kumar, Plasma Phys. Control. Fusion **61**, 025013 (2019).
[32] E. N. Nerush, I. Y. Kostyukov, A. M. Fedotov, N. B. Narozhny, N. V. Elkina, and H. Ruhl, Phys. Rev. Lett. **106**, 035001 (2011).
[33] S. S. Bulanov, C. B. Schroeder, E. Esarey, and W. P. Leemans, Phys. Rev. A **87**, 062110 (2013).
[34] M. Jirka, O. Klimo, S. V. Bulanov, T. Z. Esirkepov, E. Gelfer, S. S. Bulanov, S. Weber, and G. Korn, Phys. Rev. E **93**, 023207 (2016).
[35] A. Gonoskov, A. Bashinov, S. Bastrakov, E. Efimenko, A. Ilderton, A. Kim, M. Marklund, I. Meyerov, A. Muraviev, and A. Sergeev, Phys. Rev. X **7**, 041003 (2017).
[36] E. S. Efimenko, A. V. Bashinov, A. A. Gonoskov, S. I. Bastrakov, A. A. Muraviev, I. B. Meyerov, A. V. Kim, and A. M. Sergeev, Phys. Rev. E **99**, 031201(R) (2019).
[37] P. A. M. Dirac, Math. Proc. Cambridge Philos. Soc. **26**, 361 (1930).
[38] W. Greiner and J. Reinhardt, *Quantum Electrodynamics* (Springer Science & Business Media, New York, 2008).
[39] A. Ilderton, B. King, and A. J. MacLeod, Phys. Rev. D **100**, 076002 (2019).
[40] D. M. Volkov, Z. Phys. **94**, 250 (1935).
[41] C. N. Harvey, A. Ilderton, and B. King, Phys. Rev. A **91**, 013822 (2015).
[42] B. King, arXiv:1908.06985.
[43] L. D. Landau, *The Classical Theory of Fields*, Vol. 2 (Elsevier, New York, 2013).